RSC Advances

PAPER

View Article Online
View Journal | View Issue

Cite this: *RSC Adv.*, 2020, **10**, 28026

A voltammetric sensor based on reduced graphene oxide-hemin-Ag nanocomposites for sensitive determination of tyrosine

Hui-Yu Zou,[ab] Xin-Yang Lu,[b] Fen-Ying Kong,*[b] Zhong-Xia Wang,[b] Heng-Ye Li,[b] Hai-Lin Fang[b] and Wei Wang*[b]

Received 5th June 2020
Accepted 11th July 2020

DOI: 10.1039/d0ra04976j

rsc.li/rsc-advances

A novel voltammetric sensor was designed and used for the determination of L-tyrosine (L-Tyr) by surface modification of a glassy carbon electrode with reduced graphene oxide-hemin-Ag (rGO-H-Ag) nanocomposites. The nanocomposites were synthesized by a facile one-pot hydrothermal method and characterized by means of transmission electron microscopy and Raman spectroscopy. The determination of L-Tyr was investigated by cyclic voltammetry and further quantified using differential pulse voltammetry. The results revealed a significant enhanced electrochemical oxidation effect for L-Tyr at the nanocomposites modified electrode. Two linear ranges from 0.1 to 100 μM and 100 to 1000 μM as well as a low detection limit of 30 nM (S/N = 3) were obtained. In addition, the sensor also demonstrated good selectivity, reproducibility and stability.

1. Introduction

L-Tyrosine (L-Tyr) or 4-hydroxyphenylalanine is one important essential amino acid for humans which is used to establish and maintain nutritional balance.[1] Its level in the human body is an indicator of health status. The lack of L-Tyr can induce albinism, hypochondrium, depression, and other psychological diseases,[2] while an excess of L-Tyr results in increased sister chromatid exchange.[3] Thus, simple and sensitive determination of L-Tyr is very important for clinical diagnosis and treatment. Up to now, many methods have been reported for the determination of L-Tyr, including chromatography,[4,5] spectrophotometry,[6] fluorimetry,[7] chemiluminescence[8] and electrochemical methods.[9,10] Among them, the electrochemical sensors are more suitable for routine analysis of L-Tyr because of their characteristics of sensitivity, simplicity, selectivity and ease of on-site determination.[11–13] With rapid development in nanotechnology, nanomaterial based electrochemical sensors have been detailed studied. Various nanomaterials have been modified onto the electrodes for determination of L-Tyr, such as carbon nanofibers,[14] CeO_2 nanoparticles (NPs),[15] Au NPs,[16] graphene nanowalls,[17] *etc.* Unfortunately, the linear range, detection limit and stability still remain to be challenged. So, developing new functional nanomaterials for determination of L-Tyr with enhanced performance is highly desirable.

The recent increase of attention in graphene-based nanomaterials has opened new avenues for developing novel functional nanomaterials. The unique two-dimensional plane structure of graphene makes it promising candidate as a scaffold to anchor noble metal NPs.[18] The graphene/noble metal nanomaterials have offered greater versatility as promoted sensing material for constructing electrochemical sensors.[19] On the other hand, the incorporation of graphene with redox mediator (hemin, ferrocene, *et al.*) can obtain highly electroactive materials and can further improve the electrochemical performances of the developed sensors.[20] So, there is a reason to expect that the integration of graphene, hemin and Ag NPs into hybrid nanostructure will achieve enhanced performance for electrochemical determination of L-Tyr.

Herein, we have synthesized reduced graphene oxide-hemin-Ag (rGO-H-Ag) nanocomposites by a facile one-pot hydrothermal method and investigated its performance for voltammetric determination of L-Tyr (Scheme 1). The rGO-H-Ag nanocomposites were prepared by directly heating GO, hemin and $AgNO_3$ under alkaline conditions. The structure, morphology and phase formation characterization revealed the formation of nanocomposites in the presence of all precursors. The electrochemical test indicated favorable electrocatalytic activity towards L-Tyr oxidation. Based on the rGO-H-Ag nanocomposites modified glassy carbon electrode (rGO-H-Ag/GCE), satisfactory performances with respect to wide linear range, low detection limit, excellent selectivity and high stability for the determination of L-Tyr were achieved.

[a]*School of Chemistry and Chemical Engineering, Jiangsu University, Zhenjiang 212013, China*

[b]*School of Chemistry and Chemical Engineering, Yancheng Institute of Technology, Yancheng 224051, China. E-mail: kongfy@ycit.edu.cn; wangw@ycit.edu.cn; Fax: +86-515-88298186; Tel: +86-515-88298186*

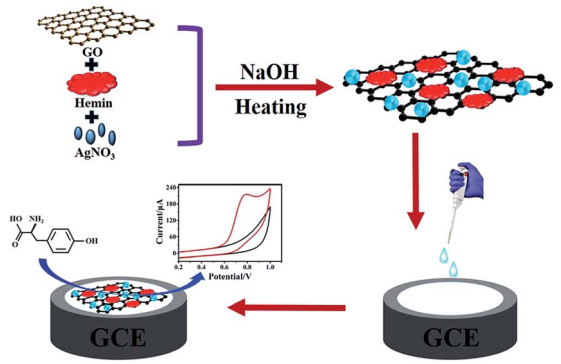

Scheme 1 Schematic of the preparation of rGO-H-Ag nanocomposites for the voltammetric determination of L-Tyr.

2. Experimental section

2.1. Materials and reagents

Graphite powder, L-Tyr and $AgNO_3$ were purchased from Aladdin Reagent Co. Ltd. Hemin (iron protoporphyrin chloride, 98 wt%) was bought from Sigma. All other chemicals were of analytical reagent grade and used as received without further purification. Stock solution of L-Tyr (1.0 mM) was prepared daily by dissolving the right amount of L-Tyr in dilute HCl. Phosphate buffer (PB) employed as a supporting electrolyte was prepared from NaH_2PO_4 and Na_2HPO_4 and the pH was adjusted with H_3PO_4 or NaOH. All aqueous solutions were prepared using ultrapure water from a Milli-Q Plus system (Millipore). All experiments were performed in accordance with the Guidelines established by the National Institutes of Health and approved by the ethics committee at Yancheng Institute of Technology. Informed consents were obtained from human participants of this study.

2.2. Apparatus

Transmission electron microscopy (TEM) images were made on a JEOL mode 2000 instrument with an accelerating applied potential of 200 kV. Raman spectra were implemented on a LabRAM HR 800 Raman spectrophotometer with 532 nm wavelength excitation laser light. All electrochemical experiments were measured on a CHI 840C electrochemical workstation at room temperature. A conventional three-electrode system was used with a 3 mm modified GCE as the working electrode, KCl saturated Ag/AgCl as the reference electrode and a platinum wire as the auxiliary electrode.

2.3. Synthesis of rGO-H-Ag nanocomposites

The rGO-H-Ag nanocomposites were synthesized by a facile one-pot hydrothermal method and the detailed experimental procedure is as follows. 10 mL of 1.0 mg mL^{-1} GO dispersion (synthesized by a modified Hummers' method as described in our previous work[21]) was mixed with 10 mL of 1.0 mg mL^{-1} hemin (dissolved in ethanol) and ultrasonic stirred for 1 h. Then, 0.1 mL 0.05 M $AgNO_3$ was added into the mixture, followed by the addition of 0.5 M NaOH solution slowly until pH was 10.0. After vigorous shaking and sonicating for 30 min at room temperature, the mixture was transferred into the flask and placed in an oil bath at 90 °C with refluxing for 1 h. After that, the production was collected by centrifugation and washed several times with water. The obtained precipitate was then dispersed in water and stored at 4 °C for further experiments.

2.4. Electrode preparation and modification

GCE was first polished with 0.3 and 0.05 μm alumina slurry to a mirror-like finish. Then, it was rinsed thoroughly with water, followed by sonication in ethanol and water for 5 min, respectively. Finally, GCE was dried under a stream of nitrogen. For the preparation of rGO-H-Ag/GCE, 5 μL of rGO-H-Ag dispersion was cast onto the surface of the pretreated GCE and allowed to dry at room temperature.

2.5. Experimental procedure

10 mL of solution containing 0.2 M PB and suitable amounts of L-Tyr was firstly transferred to the electrochemical cell. Then, the three-electrode system was inserted into it through a plastic Teflon. After deaerated by nitrogen gas for 15 min and maintained a nitrogen atmosphere over the solution, the cyclic voltammograms (CVs) were measured from 0.2 to 1.0 V at a scan rate of 100 mV s^{-1}. The oxidation peak current at 0.78 V was recorded as the analytical signal for L-Tyr. The differential pulse voltammograms (DPVs) were obtained at a scan rate of 100 mV s^{-1}, 50 mV pulse amplitude and 200 ms pulse interval.

3. Results and discussion

The rGO-H-Ag nanocomposites were synthesized *via* a simple hydrothermal method and the obtained rGO-H-Ag nanocomposites were applied to voltammetric determination of L-Tyr. Scheme 1 demonstrates the preparation of rGO-H-Ag nanocomposites and the determination of L-Tyr. In the preparation process, hemin firstly anchored on the surface of GO sheets through π–π interaction. Then, the conjugated GO-H serves as a scaffold to anchor Ag NPs. At the same time, GO can be reduced into rGO under strong alkaline condition. Subsequently, the rGO-H-Ag nanocomposites were coated onto the surface of GCE to investigate its performance for electrochemical determination of L-Tyr. Hemin not only showed excellent direct electrochemistry, but also could oxidize L-Tyr.[22] On the other hand, rGO can promote the electron transfer kinetics and electrocatalytic activity. In addition, Ag NPs have fascinating catalytic activity. Thus, combination the merits of each component in the rGO-H-Ag nanocomposites, a high sensitivity electrochemical sensor for the determination of L-Tyr was achieved.

3.1. Characterizations of the rGO-H-Ag nanocomposites

To confirm the successful preparation of the rGO-H-Ag nanocomposites, TEM images and Raman spectroscopy were used. Fig. 1 shows the typical TEM images of GO, rGO-H and rGO-H-Ag nanocomposites, respectively. As can be seen, GO exhibits a flake-like shape with crumpled and wrinkled surface (Fig. 1A).

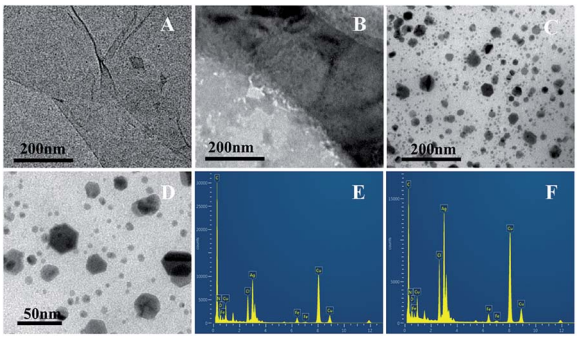

Fig. 1 Typical TEM images of GO (A), rGO-H (B), low (C) and high (D) magnification images of rGO-H-Ag nanocomposites; the EDX spectra of different sized particles (E and F) over the rGO surface.

This structure provides a large surface as scaffold for hemin and Ag NPs loading. In Fig. 1B, some aggregates appear on the surface of rGO and the surface of rGO is not smooth.

The aggregates may be caused by the adsorption of hemin through π–π interactions.[23] Fig. 1C and D demonstrate the images of rGO-H-Ag nanocomposites at low and high magnifications. Low magnification image shows that a large number of NPs are densely covered on the surface of rGO-H. The size and shape of these NPs are not the same. A high magnification image indicates that the smaller NPs are mostly spherical in shape with the diameter of 6 nm and the bigger NPs are nearly hexagons in shape. The chemical composition of the different sized particles over the rGO surface was determined by EDX (Fig. 1E and F). The spectra show the peaks corresponding to C, O, Cl, N, Fe, Cu and Ag elements, confirming the existence of metallic Ag onto the surface of the rGO. The observed Fe, Cl and N peaks represents the existence of hemin on the surface of the rGO.

Fig. 2 shows the Raman spectra of GO (curve a), hemin (curve b) and rGO-H-Ag nanocomposites (curve c). As can be seen, GO shows a D band at 1351 cm^{-1} and a G band at 1594 cm^{-1}. The D band and G band are related to the vibration of sp^3-bond carbon atoms of disordered graphene sheet and the sp^2-bonded carbon atoms domains of graphite, respectively. The intensity ratio (I_D/I_G) is greatly influenced by the defect level in the atomic carbon structure.[24] For the Raman spectra of hemin, three major bands located at 1636 cm^{-1}, 1590 cm^{-1}, and 1382 cm^{-1} can be clearly observed, which are ascribed to the asymmetric C–C stretching and the symmetric pyrrole-half-ring stretching of the protoporphyrin (IX) ring system.[25] After the formation of rGO-H-Ag nanocomposites, besides the three characteristic bands of hemin can be seen, the I_D/I_G increased compared with pure GO, indicating the successful attachment of hemin onto GO sheet and the conversion of GO into rGO.[26]

The electrochemical characteristics of the rGO-H-Ag/GCE were subsequently investigated. Fig. 3A shows the CVs recorded in 0.2 M N_2-saturated PB (pH 7.0) at rGO-H/GCE (curve a) and rGO-H-Ag/GCE (curve b). A pair of obvious redox peaks is observed at the rGO-H/GCE in the potential range from −1.0 V to 0.2 V. The peaks should be attributed to the Fe(III)/Fe(II) redox couple coordinated in the porphyrinic ring,[27] revealing that hemin was adhere on the surface of rGO. By contrast, a greatly improved redox peak currents of hemin is displayed at the rGO-H-Ag/GCE, demonstrating that the Ag NPs are acting as a catalytic enhancer on the surface of the rGO-H. In addition, Fig. 3B shows the CV of rGO-H-Ag/GCE recorded in a wider potential range. A well-defined oxidation peak at about 0.27 V and a small reduction peak at *ca.* 0.01 V corresponding to the redox of Ag NPs was observed. The appearance of typical characteristics of Ag NPs witness the attachment of Ag NPs in the nanocomposites.

Furthermore, the effect of scan rate on the CV performance of rGO-H-Ag/GCE was also evaluated. Fig. 4A presents typical CVs of rGO-H-Ag/GCE at different scan rates (100 to 1000 mV s^{-1}) recorded in N_2-saturated 0.2 M PB (pH 7.0). As illustrated, the redox peaks grow continuously with increasing the scan rate. Good linear relationships can be observed between the redox peaks current and scan rate from 100 to 1000 mV s^{-1}, as shown in Fig. 4B. The linear regression equations were I_{pa} (μA) = 9.238 + 0.06998 (mV s^{-1}) (R^2 = 0.9969) and I_{pc} (μA) = −20.718 − 0.09682 (mV s^{-1}) (R^2 = 0.9925), revealing that the redox reaction of hemin on the rGO-H-Ag/GCE is a surface-controlled electrochemical process.[28]

3.2. Electrochemical behavior of L-Tyr at rGO-H-Ag/GCE

The electrochemical behaviour of L-Tyr was studied in 0.2 M pH 7.0 PB by CV and the results are shown in Fig. 5. As can be seen, in the selected potential region, there is no redox peaks in the absence of L-Tyr (curve a). When 0.2 mM L-Tyr was added into the buffer, a distinct oxidation peak at around 0.78 V is observed at rGO-H-Ag/GCE (curve b). In the reverse scan, no any reduction peak appeared, suggesting that the electrochemical reaction of L-Tyr is totally irreversible process.

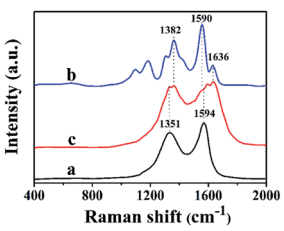

Fig. 2 Raman spectra of GO (a), hemin (b) and rGO-H-Ag nanocomposites (c).

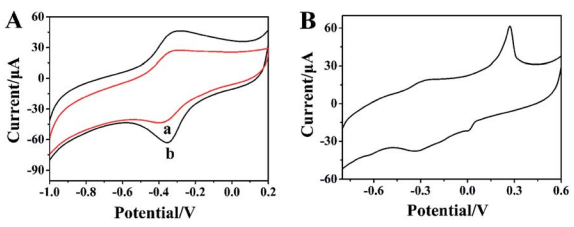

Fig. 3 CVs of rGO-H/GCE (a) and rGO-H-Ag/GCE (b) in N_2-saturated 0.2 M pH 7.0 PB (A); CVs of rGO-H-Ag/GCE in N_2-saturated 0.2 M pH 7.0 PB (B). Scan rate: 100 mV s^{-1}.

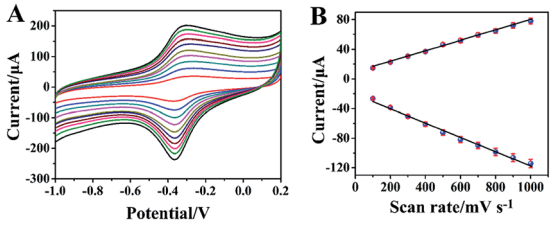

Fig. 4 CVs of rGO-H-Ag/GCE in N_2-saturated 0.2 M pH 7.0 PB at different scan rates (inner to outer) 100, 200, 300, 400, 500, 600, 700, 800, 900 and 1000 mV s^{-1} (A); plots of oxidation and reduction peak currents *vs.* scan rate (B).

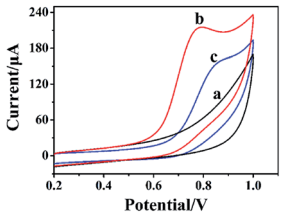

Fig. 5 CVs of rGO-H-Ag/GCE in the absence (a) and presence (b) of 0.2 mM L-Tyr in N_2-saturated 0.2 M pH 7.0 PB, and CV of rGO-H/GCE in the presence of 0.2 mM L-Tyr in N_2-saturated 0.2 M pH 7.0 PB (c). Scan rate: 100 mV s^{-1}.

In contrast, the rGO-H/GCE shows a weak oxidation peak at a relatively high potential of 0.85 V (curve c). The enhancement in peak current and the decrease in peak potential revealed that the ternary nanocomposite of rGO-H-Ag can effectively catalyze the electrochemical oxidation of L-Tyr. It is ascribed to the huge specific surface area and superior electrical conductivity of rGO-H-Ag nanocomposites, which can increase the effective area of the electrode and improve the electron transfer rate.[29–32]

3.3. DPV determination of L-Tyr at rGO-H-Ag/GCE

Due to DPV owns high sensitivity and excellent resolution, the analytical determination of L-Tyr was performed using DPV. Fig. 6 presents a series of DPVs of rGO-H-Ag/GCE in N_2-saturated 0.2 M pH 7.0 PB with increasing L-Tyr concentration (A) and its corresponding calibration plots (B). As illustrated, the oxidation peak currents increase with the increasing

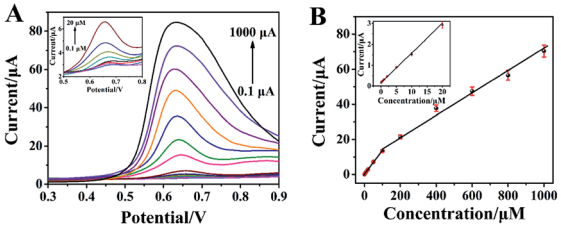

Fig. 6 DPVs of various concentration of L-Tyr (from bottom to top, 0.1–1000 μM) at rGO-H-Ag/GCE in N_2-saturated 0.2 M pH 7.0 PB (A), the calibration plots of oxidation peak current *vs.* L-Tyr concentration (B). Inset: DPVs (A) and calibration plots (B) for L-Tyr with low concentrations (0.1–20 μM).

concentrations of L-Tyr. Good linear relationships are observed between the oxidation peak currents and L-Tyr concentrations in two ranges from 0.1 to 100 μM and 100 to 1000 μM, respectively. The corresponding regression equations are I (μA) = 0.2118 + 0.1344c (μM) (R^2 = 0.9990) and I (μA) = 9.5916 + 0.06117c (μM) (R^2 = 0.9872). Inset (A) and (B) in Fig. 6 show the magnified DPVs and calibration plots for L-Tyr with low concentrations (0.1–20 μM) to make them more clarity. The limit of detection was calculated to be 30 nM based on the signal-to-noise ratio of 3 using the calibration equation obtained for low concentration range. Note that our proposed rGO-H-Ag/GCE provided a broader linear range than that of SWCNH/GCE (2–30),[29] CuO/Cu_2O/MWCNTs/GCE (0.2–200),[31] PTH/AGCE (1–250),[33] Nafion/TiO_2-GR/GCE (10–160),[34] GR/GCE (0.8–60),[35] GQD-$RuCl_3$/CCE (1–937)[36] and PAMAM/MWCNT/GCE (0.1–28.8)[37] listed in Table 1. The enhanced performance of the rGO-H-Ag nanocomposites can be ascribed to the large specific surface area, high electrocatalytic activity, good electrical conductivity, fast electron transfer and the synergistic interaction of three components. Thus, the rGO-H-Ag/GCE is an ideal platform for the electrochemical determination of L-Tyr.

3.4. Selectivity, reproducibility and stability of the rGO-H-Ag/GCE

In order to assess the selectivity of rGO-H-Ag/GCE, the experiment was conducted in 0.2 M pH 7.0 PB containing 0.2 mM L-Tyr and various potentially interferents. The results indicated that 100-fold concentration of glucose, sucrose, fructose, alanine, glycine, lysine, histidine, phenylalanine, folic acid had no obvious influence on the peak current of 0.2 mM L-Tyr (peak current change < 5%). In addition, some inorganic ions such as 500-fold concentration of K^+, Na^+, Mg^{2+}, Al^{3+}, Cu^{2+}, Fe^{3+}, Ca^{2+}, Cl^-, NO_3^-, SO_4^{2-}, did not interfere with the determination of 0.2 mM L-Tyr. All these results revealed that the rGO-H-Ag/GCE has good selectivity for the determination of L-Tyr.

To demonstrate the reproducibility of rGO-H-Ag/GCE, six successive measurements were carried out in the presence of 0.2 mM L-Tyr by using the same electrode. The values of relative standard deviation (RSD) was calculated to be 4.1%. Five different rGO-H-Ag/GCEs fabricated independently under the same conditions had a small deviation (RSD 5.9%) in the peak currents, confirming the excellent reproducibility of rGO-H-Ag/GCE. The stability of rGO-H-Ag/GCE was performed by measuring 100 cycles of CVs. No obvious decrease in peak current was observed between the first CV and 100th CV. In addition, the long-term stability of the rGO-H-Ag/GCE was investigated after storing 15 days in a refrigerator at 4 °C. The peak current remained 92.1% of the original value, indicating the good stability of rGO-H-Ag/GCE. The excellent selectivity, reproducibility and stability of rGO-H-Ag/GCE make it attractive for practical application.

3.5. Real samples analysis

The rGO-H-Ag/GCE was finally applied for determination of L-Tyr in human urine samples using DPV technology. The human urine samples were collected from three healthy adults and

Table 1 Comparison of the performances of different modified electrodes for the determination of L-Tyr[a]

Electrode	Method	Linear range (μM)	Detection limit (μM)	Ref.
SWCNH/GCE	LSV	2–30	0.4	29
CuO/Cu_2O/MWCNTs/GCE	LSV	0.2–200	0.0096	31
PTH/AGCE	DPV	1–250	0.57	33
Nafion/TiO_2-GR/GCE	DPV	10–160	2.3	34
GR/GPE	SWV	0.8–60	0.07	35
GQD-$RuCl_3$/CCE	*i–t*	1–937	0.23	36
PAMAM/MWCNT/GCE	*i–t*	0.1–28.8	0.01	37
rGO-H-Ag/GCE	DPV	0.1–100, 100–1000	0.03	This work

[a] PTH/AGCE: poly(thionine)-modified anodized glassy carbon electrode; SWCNH: single-walled carbon nanohorns; GR/GPE: graphene modified graphite pencil electrode; GQD: graphene quantum dot; CCE: carbon-composite electrode; PAMAM: poly amidoamine.

Table 2 Determination of L-Tyr in human urine samples at rGO-H-Ag/GCE ($n = 3$)

Sample Number	Added (μM)	Found (μM)	Recovery (%)
1	50.0	48.8	97.6
2	100	99.4	99.4
3	200	208	104

diluted to 10 times with 0.2 M pH 7.0 PBS. Afterward, all the sample solutions were transferred into the electrochemical cell and L-Tyr was determined using the standard addition method. The results are presented in Table 2. It is clear that the recoveries are in the range of 97.6–104% ($n = 3$ repetitions) with acceptable range, revealing that the rGO-H-Ag/GCE can be efficiently used for the determination of L-Tyr in real sample.

4. Conclusions

In summary, an electrochemical sensor for sensitive determination of L-Tyr was developed based on the rGO-H-Ag nanocomposites. In the electrochemical measurement process, the rGO and Ag NPs facilitated the electron transfer between the hemin and the electrode while the hemin effectively catalyzed the oxidization of L-Tyr. Thus, the excellent synergic effect of each components in the rGO-H-Ag nanocomposites enabled an improved electrochemical performance for the determination of L-Tyr with satisfactory linear range (0.1–100 μM, 100–1000 μM), low detection limit (30 nM), good selectivity and high stability. The proposed L-Tyr sensor offers potential applications in pharmaceutical, clinical, environmental, and other analytical fields.

Conflicts of interest

There are no conflicts to declare.

Acknowledgements

This work was supported by the National Natural Science Foundation of China (21675139, 21705140, 21876144, 21974120), the Natural Science Foundation of Jiangsu Province (BK20170474, BK20191479), and Qing Lan Project of Jiangsu universities.

Notes and references

1 H. F. Femstrom and J. D. Femstrom, *Life Sci.*, 1995, **57**, 97.
2 Ö. A. Yokus, F. Kardas, O. Akyıldırım, T. Eren, N. Atar and M. L. Yola, *Sens. Actuators, B*, 2016, **233**, 47.
3 S. Zhou, H. Wu, Y. Wu, H. Shi, X. Feng, H. Huang, J. Li and W. Song, *Electrochim. Acta*, 2013, **112**, 90.
4 D. I. Sánchez-Machado, B. Chavira-Willys and J. López-Cervantes, *J. Chromatogr. B: Anal. Technol. Biomed. Life Sci.*, 2008, **863**, 88.
5 C. Deng, Y. Deng, B. Wang and X. H. Yang, *J. Chromatogr. B: Anal. Technol. Biomed. Life Sci.*, 2002, **780**, 407.
6 Y. Azuma, M. Maekawa, Y. Kuwabara, T. Nakajima, K. Taniguchi and T. Kanno, *Clin. Chem.*, 1989, **35**, 1399.
7 F. Wang, K. Z. Wu, Y. Qing and Y. X. Ci, *Anal. Lett.*, 1992, **25**, 1469.
8 C. Y. Gao and S. H. Fan, *Anal. Lett.*, 2014, **47**, 178.
9 M. Hasanzadeh, S. Sadeghi, L. Bageri, A. Mokhtarzadeh, A. karimzadeh, N. Shadjou and S. Mahboob, *Mater. Sci. Eng., C*, 2016, **69**, 343.
10 L. J. Zeng, H. Wang, X. J. Bo and L. P. Guo, *J. Electroanal. Chem.*, 2012, **687**, 117.
11 S. Shrestha, R. J. Mascarenhas, O. J. D'Souza, A. K. Satpati, Z. Mekhalif, A. Dhason and P. Martis, *J. Electroanal. Chem.*, 2016, **778**, 32.
12 H. Razmi, H. Nasiri and R. Mohammad-Rezaei, *Microchim. Acta*, 2011, **173**, 59.
13 P. Kanchana, N. Lavanya and C. Sekar, *Mater. Sci. Eng., C*, 2014, **35**, 85.
14 X. Tang, Y. Liu, H. Hou and T. You, *Talanta*, 2010, **80**, 2182.
15 A. S. Razavian, S. M. Ghoreishi, A. S. Esmaeily, M. Behpour, L. M. A. Monzon and J. M. D. Coey, *Microchim. Acta*, 2014, **181**, 1947.
16 H. Cheng, C. Chen and S. Zhang, *Anal. Sci.*, 2009, **25**, 1221.
17 F. Y. Tian, H. J. Li, M. J. Li, C. P. Li, Y. J. Lei and B. H. Yang, *Microchim. Acta*, 2017, **184**, 1611.

18 W. W. Li, F. Y. Kong, J. Y. Wang, Z. D. Chen, H. L. Fang and W. Wang, *Electrochim. Acta*, 2015, **157**, 183.
19 F. Y. Kong, L. Yao, R. F. Li, H. Y. Li, Z. X. Wang, W. X. Lv and W. Wang, *J. Alloys Compd.*, 2019, **797**, 413.
20 N. Xia, L. Liu, Z. F. Sun and B. B. Zhou, *J. Nanomater.*, 2015, **2015**, 892674.
21 F. Y. Kong, W. W. Li, J. Y. Wang and W. Wang, *Biosens. Bioelectron.*, 2015, **69**, 206.
22 J. H. Wei, J. J. Qiu, L. Li, L. Q. Ren, X. W. Zhang, J. Chaudhuri and S. R. Wang, *Nanotechnology*, 2012, **23**, 335707.
23 R. Jiang, D. T. Tran, J. McClure and D. Chu, *Electrochem. Commun.*, 2012, **19**, 73.
24 F. Y. Kong, R. F. Li, L. Yao, Z. X. Wang, H. Y. Li, W. J. Wang and W. Wang, *Nanotechnology*, 2019, **30**, 285502.
25 W. J. Huang, Q. L. Hao, W. Lei, L. H. Wu and X. F. Xia, *Mater. Res. Express*, 2014, **1**, 045601.
26 W. Wei, D. M. Zhang, L. H. Yin, Y. P. Pu and S. Q. Liu, *Spectrochim. Acta, Part A*, 2013, **106**, 163.
27 X. D. Cao, J. N. Gao, Y. W. Ye, P. F. Wang, S. Ding, Y. K. Ye and H. J. Sun, *Electroanal*, 2016, **28**, 140.
28 F. P. Liu, J. Q. Tang, J. Xu, Y. Shu, Q. Xu, H. M. Wang and X. Y. Hu, *Biosens. Bioelectron.*, 2016, **86**, 871.
29 S. Y. Zhu, J. Zhang, X. E. Zhao, H. Wang, G. B. Xu and J. M. You, *Microchim. Acta*, 2014, **181**, 445.
30 K. J. Huang, L. Wang, H. B. Wang, T. Gan, Y. Y. Wu, J. Li and Y. M. Liu, *Talanta*, 2013, **114**, 43.
31 W. X. Gu, M. M. Wang, X. Q. Mao, Y. R. Wang, L. Li and W. S. Xia, *Anal. Methods*, 2015, **7**, 1313.
32 M. Amiri, M. Salavati-Niasari and A. Akbari, *Microchim. Acta*, 2017, **184**, 825.
33 M. M. Rahman, N. S. Lopa, K. Kim and J. J. Lee, *J. Electroanal. Chem.*, 2015, **754**, 87.
34 Y. Fan, J. H. Liu, H. T. Lu and Q. Zhang, *Microchim. Acta*, 2011, **173**, 241.
35 N. Baig and A. N. Kawde, *Anal. Methods*, 2015, **7**, 9535.
36 E. Habibi and H. Heidari, *Electroanal*, 2016, **28**, 2559.
37 Q. Ma, S. Y. Ai, H. S. Yin, Q. P. Chen and T. T. Tang, *Electrochim. Acta*, 2010, **55**, 6687.